Innervation, Distribution And Morphology Of Calcitonin Gene Related Peptide And Substancep Immunoreactive Axons In The Whole-mount Atria Of Fvb Mice

2010

Liang Li
University of Central Florida

Innervation, distribution and morphology of calcitonin gene related peptide and substance P immunoreactive axons in the whole-mount atria of FVB mice

by

LIANG LI
M.S. China Pharmaceutical University, 2006
B.S. China Pharmaceutical University, 2001

A thesis submitted in partial fulfillment of the requirements
for the degree of Master of Science
in the Department of Molecular Biology and Microbiology
in the Burnett School of Biomedical Sciences
in the College of Medicine
at the University of Central Florida
Orlando, Florida

Fall Term
2010

ABSTRACT

Degeneration of nociceptive afferent axons and terminals in the heart is associated with painless sudden cardiac death. However, innervation, distribution and morphological structures of sympathetic cardiac nociceptive afferent axons and terminals have not yet been fully characterized. The aim of the present study is to characterize the density, arrangement, and structural features of differentiated sympathetic afferent axons and terminals in whole-mount FVB mouse atria. FVB mice (3-6 months old) were perfused and the tissues were fixed. The right and left atria were processed with immunohistochemistry. Calcitonin gene-related peptide (CGRP) and substance P (SP) are two neuropeptides which have been widely used to label sympathetic nociceptive afferent axons in many tissues. CGRP (rabbit anti-CGRP) and SP (Goat anti-SP) primary antibodies were applied, followed by Alexa Fluor 594 and 660 conjugated secondary antibodies. Whole-mount preparations of right and left atria were examined using a laser scanning confocal microscope. We found that 1) CGRP immunoreactive (IR) axon bundles innervated the right and left atria including the auricle and entrance area of the superior vena cava, the inferior vena cava, left precaval vein and pulmonary veins. Large axon bundles entered the area from the major veins and bifurcated into smaller axon bundles and single axon fibers to form terminal end-nets and free endings in the epicardium at each region with a similar pattern. In the atrial muscle layer, varicose CGRP-IR axons had close contacts with muscle fibers. In addition, CGRP-IR axons

terminated in the intrinsic cardiac ganglia (ICGs) with varicosities surrounding individual ganglionic principle neurons (PNs). In the aortic arch, the CGRP-IR fibers exhibited similar terminal structures to those seen in the atria. 2) SP-IR axons also projected to the right and left atria and aorta. Similar to CGRP-IR axons, these SP-IR axons also formed end-nets and free endings in these areas. In cardiac ganglia, SP-IR axons formed varicose endings around many individual PNs. However, a salient difference was found: There appeared to be fewer SP-IR axons and terminals than CGRP-IR axons and terminals in the atria. 3) None of the cardiac PNs in ICG were CGRP-IR or SP-IR. 4) Many SP-IR axon terminals around PNs within ICGs and atrial muscles were found to have colocalized expression of CGRP-IR. Collectively, our data for the first time documented the distribution patterns and morphology of sympathetic afferent axons and terminals in each region of the atria in the mouse model. This will provide a foundation for future analysis of the pathological changes of sympathetic afferent nerves in the atria in different disease models (e.g., diabetes, sleep apnea, and aging). This study was supported by NIH R01 HL-79636.

ACKNOWLEDGMENTS

I would like to express my sincere thanks to my committee: Dr. Ella Bossy-Wetzel, Dr. Sic L. Chan and Dr. Mohtashem Samsam for their constructive suggestions and insightful comments on my thesis.

My heartfelt thanks also go to my lab members: Lihua Li, for teaching me the delicate microsurgical and tissue dissecting skills; Scott Harden for his talented confocal imaging skills as well as patiently helping me improve my English; Jeffery Hatcher for attentively editing my thesis; Drs. Xueguo Zhang, Binbin Yan, and He Gu for thoroughly walking me through the electrophysiological techniques; Drs. He Gu and Binbin Yan for their warm, generous support and instructing me in general lab skills.

I am especially grateful to my advisor, Dr. Zixi (Jack) Cheng for providing me with the highest quality research training. He guided me step by step throughout my graduate student career: scholastics, critical analysis of the literature, mentoring me on how to be a more careful and conscientious researcher, and all his helpful suggestions and criticisms for my Thesis. In addition, he spent a lot of time teaching me English as well as presentation skills, which is of great importance to me for building my self-confidence. Finally, he set a great example of finding the balance between work and everyday life. I enjoyed every minute with him and have learned many things that will benefit me throughout my whole life.

My deepest thanks also go to my parents and my aunt who have unselfishly supported and encouraged me in my academic career, and whose values and love have guided me while I was far from home.

Last but not least, I give thanks to my wife who has been my greatest inspiration and closest friend. She has lovingly supported me through many difficult times. Without her, it would not have been possible for me to accomplish my thesis.

TABLE OF CONTENTS

LIST OF FIGURES

LIST OF ACRONYMS / ABBREVIATIONS

CGRP	Calcitonin Gene Related Peptide
SP	Substance P
IR	Immunoreactivity
ICG	Intrinsic Cardiac Ganglion
ICGN	Intrinsic Cardiac Ganglionic Neurons
PN	Principal Neuron
IHC	Immunohistochemical / Immunohistochemistry
PBS	Phosphate-Buffered Saline
ZF	Zamboni's Fixative
CM	Circular Muscle
MG	Myenteric Ganglia
ACh	Acetylcholine

INTRODUCTION

Silent cardiac ischemia is a deadly serious condition that frequently occurs in the patients with cardiac failure, with advanced age, and after long-term diabetes (Faerman et al., 1977; Gutterman, 2009). Although the exact underlying mechanism for this devastating event is not clear, it is apparently related to cardiac nociceptive nerve degeneration (Faerman et al., 1977, Ambepityia et al., 1990; Langer et al, 1991). Therefore, it is critically important to characterize the remodeling of sympathetic nociceptive nerves in cardiac tissue. However, innervation, distribution and morphology of sympathetic nociceptive fibers and terminals have not yet been completely elucidated, which has seriously impeded the progress of focused investigation on diseased-induced pathological changes of sympathetic cardiac nerves. The present study aims to investigate the density, arrangement, and structural features of sympathetic nociceptive axons and terminals in whole-mount atrial tissues.

Calcitonin gene-related peptide (CGRP) and substance P are both peptidergic neurotransmitters in capsaicin-sensitive sensory nerves (Holzer, 1991; Maggi, 1995; Holzer and Maggi, 1998). The dorsal root ganglia contain both CGRP and SP sensory neurons which project centrally to the dorsal horn in the spinal cord for pain sensation, and peripherally to the heart (atria and ventricles) and other organs to detect the chemical signals (e.g., bradykinin) that are released during injuries or through transient receptor potential vanilloid (TRPV1)-mediated mechanism to induce neurogenic responses (Zahner et al., 2003; Pan and Chen, 2004; Geppetti et al., 2008; Benemei et

al., 2009; Thornton et al., 2010). Since the sensation of the pain is first detected by sympathetic (spinal) afferent terminals within the heart (Pan and Chen 2004), we focused our study on peripheral sympathetic sensory axon fibers.

In the literature, the structure and function of CGRP-IR and SP-IR neurons and axons have been examined in several different species (such as humans, dogs, cats, guinea pigs, rats, mudpuppies; (Saito A et al., 1986; Parsons and Neel, 1987; Papka and Urban, 1987; Shoba and Tay, 2000; Pan and Chen, 2002; Richardson et al., 2003; Hoover et al., 2008, 2009; Mousa et al., 2010). However, most of these studies used sectioned cardiac tissues in which axon and terminal structures have been largely damaged, leading to fragmentary views of these axons and terminals in the heart. Although whole-mount cardiac tissues were used in some studies, these studies mainly focused on some special cardiac targets, such as cardiac ganglia, again leading to an incomplete view of sympathetic afferent axons in the heart (Richardson et al., 2003; Parsons et al., 2006). In addition, all these studies were in animal models that are relatively larger than mice. No studies on CGRP-IR and SP-IR cardiac axons and terminals were found in mouse models. In the past, mice have proven to be a favorable model for the study of cardiac function and remodeling in disease states. One of the values of the mouse model is the speed and ease with which it can be genetically manipulated and bred to produce sustainable experimental populations. The size and tissue characteristics of the mouse heart make it amenable to whole-mount studies of cardiac nerve distribution which will allow for a more comprehensive, holistic (3-D) characterization of these fibers, thus providing more information than previous studies

of sectioned cardiac tissues in other species. CGRP and SP were chosen as representative markers of nociceptive nerve types because they are highly specific to nociceptive nerves, and their peptidergic nature makes them good targets for antibody probes. Therefore, the goal of the present study is to study the innervation, distribution, and morphology of the sympathetic afferent (CGRP and SP) axons and terminals in the whole-mount atria of mice.

Previously, Cheng and his colleagues studied parasympathetic afferent and efferent axons and terminals in the atria and aortic arch in normal and disease models (aging, sleep apnea and diabetes) (Cheng et al. 1997a,b; 2004; Cheng and Powley 2000; Ai et al. 2007, 2009; Lin et al. 2008; Li et al. 2010). Recently, Cheng's group has studied sympathetic efferent innervation in normal mice (Harden et al. 2009; 2010). The present study will document the distribution, and morphology of the sympathetic afferent (CGRP and SP) axons and terminals in whole-mount atria of mice (Figure 3).

MATERIALS AND METHODS

Animals

FVB mice (n=20, age 3 - 6 months) were used. All animals were housed in a room in which light/dark cycles were set to 12 h/12 h (6:00 AM to 6:00 PM light cycle) and provided food and water ad libitum. All procedures were approved by the University of Central Florida Animal Care and Use Committee and strictly followed the guidelines established by NIH. All experiments conformed to the University of Central Florida guidelines on the ethical use of animals.

Tissue Preparation

Mice were anesthetized with a lethal dose injection of sodium pentobarbital (i.p., 100 µg/g). Absence of hind paw pinch withdrawal reflex was used as an indicator to ensure sufficient depth of anesthesia. Mice were perfused through the left ventricle with 40º C PBS (1 M phosphate-buffered saline, pH=7.4) for 5 minutes. The inferior vena-cava was cut to drain the blood for the perfusion. Tissues were then fixed by perfusion with 4º C Zamboni's fixative (15% picric acid and 2% paraformaldehyde in PBS, pH=7.4). The heart and lungs were removed (Figure 2A) together with the trachea and the esophagus to ensure the completeness of the cardiac tissues which were postfixed in 4º C Zamboni's fixative for 8-24 hours.

After postfixation, the heart and lungs were dissected apart. Briefly, the pulmonary veins were separated from the lungs with fine tweezers and the lungs and trachea were discarded (Figure 2B). Atria were separated from the ventricles with fine

scissors along the atrial-ventricular groove (Figure 2C), and the aortic arch (AA) was then separated from the atria (Figure 2D). The right and left atria were then separated along interatrial septum. The dissected specimens are as follows (Figure 2E): right atrium with the inferior vena cava (IVC), superior vena cava (SVC), and left precaval vein (LPCV) attached, left atrium with pulmonary veins (PVs) attached and aortic arch (Cheng et al. 1997; Ai et al. 2008).

Immunohistochemistry

All immunohistochemical procedures were performed on a shaker at room temperature (75oF) in a 24 well plate (free floating method). Dissected tissues were washed 6 x 5 minutes (6 times, 5 minutes each) in 0.01 M PBS pH=7.4 to remove the remaining fixative. Tissues were then blocked 5 days in a blocking mixture containing 2% bovine serum albumin, 10% normal donkey serum, 0.08% Triton X-100, 0.08% NaNH3 in 0.01 M PBS, pH=7.4, followed by a 24 hour primary antibody incubation (CGRP, 1:1000; Substance P, 1: 500) (Table 1) in the solution (2% bovine serum albumin, 4% normal donkey serum, 0.08% Triton X-100, 0.05% NaNH3 in 0.01 M PBS, pH=7.4). The tissues were thoroughly washed 6 x 5 minutes in PBST (0.4% Triton X-100 in 0.01 M PBS) to remove unbound primary antibodies. Tissues were then kept in dark room and incubated in a secondary antibody solution (1:500 secondary antibody in PBST) (Table 1) for 2 hours. 6 x 5 min washes in PBS were then used to remove unbound secondary antibodies. Negative controls without primary antibodies were

performed. Negative controls presented no immunoreactivity, confirming that nonspecific binding of secondary antibodies did not occur.

Tissues were then mounted with their cranial surface up onto positively-charged glass slides, crushed with lead weights for 1 hour, and air-dried under a fume hood for 1 hour. Slides were dehydrated by immersion for 2 minutes in each of 4 ascending concentrations of ethanol (75%, 95%, 100% and 100%), followed by 2x10 min immersions in 100% xylene. Slides were then coverslipped with DEPEX mounting medium (Electron Microscopy Sciences #13514) and allowed to dry overnight. Tissues were never allowed to dry except during the air drying step.

Data collection and analysis

Slides were examined using a Leica SP5 laser scanning confocal microscope (objective: 20X oil) with HeNe laser (543 nm) for CGRP-IR axons and HeNe laser (633nm) for SP-IR axons to show the overall innervation of CGRP-IR and SP-IR axons in the whole-mount atria. The argon-krypton laser (488nm) was used to detect the autofluorescence of the tissues (e.g., cardiac muscles and ganglionic cells) in the background. The confocal projection images for assembling the montage of the atria and the aortic arch which were scanned using a 20x oil immersion objective lens (zoom X1). To show detailed CGRP-IR and SP-IR axon distribution in the heart, confocal optical sectioned images were scanned using a 40x oil immersion objective lens (zoom X2).

All confocal images were scanned with the similar settings. Modifications, including brightness and contrast adjustments, cropping and scale bar additions were conducted utilizing Photoshop or NIH ImageJ (Collins, 2007) software.

Confocal montages were assembled using the landmark-based method for efficient, robust, and automated computational synthesis of high-resolution, wide-area images of a specimen from a series of overlapping partial views (Becker et al, 1996). Individual scans of a small window with a certain size were first obtained and saved in stacks of optical sectioned images. Then, these stacks were maximally-projected to yield a series of all-in-focus maximum projection tiles. MosaicJ (Thévenaz and Unser, 2007) was utilized to assist in the assembly of these tiles to create large montage images. Artifacts (air bubbles trapped in the mounting media) were manually removed from the resulting images, but primarily outside of the perimeter of the tissue, and never in the regions selected for representative image presentation.

RESULTS

Innervation, distribution and morphology of CGRP-IR axon and terminals in whole-mount atria

The whole-mount nature of atrial preparations allowed for the assessment of CGRP-IR axon innervation in the right and left atria of a representative mouse (Figure 3 and 4, respectively). Although the distribution of CGRP-IR fibers was complex and some variations in structural details were observed across animals, the general scheme of CGRP-IR nerve distribution patterns were similar in all animals studied. This is shown in the schematic drawing of this representative animal (Figure 5). In both right and left atria (Figures 3, 4, and 5), large bundles of CGRP-IR axons, likely from the dorsal root ganglia near the spinal cord, (see discussion) entered the atria. The large bundles bifurcated multiple times into fine individual axons which formed extensive terminal end-nets and free endings over the entire atria including the auricles and the entrance areas of several major veins (Figures 6 and 8). The terminal end-nets were mostly in the epicedium, where the fine axons were intermingled with the cardiac muscles in the myocardium (Figure 7).

As reported before (Ai et al. 2007; Lin et al. 2008), a total of 15-20 intrinsic cardiac ganglia of different sizes were found in the dorsal surface of the right and left atria (Figure 5). CGRP fibers traveled in the connectives of these ganglia (Figure 9). Some of CGRP-IR axons formed dense varicose endings around individual PNs in ICGs, whereas others appeared passing by the ICGs (Figures 9 and 10). CGRP

immunoreactivity was observed in numerous nerve fibers but was not found within the somata of cardiac principle neurons (PNs) in our tissue. It appeared that innervation, distribution and morphology of CGRP-IR axons in different areas of the right and left atria followed a similar pattern.

CGRP-IR innervation of the whole-mount aortic arch

CGRP-IR axons were distributed along the wall of the aortic arch. Similar to the atria, large CGRP-IR axon bundles bifurcated multiple times into single axons and formed terminal end-nets and free terminals on the surface of the aortic arch (Figure 11).

Innervation, distribution and morphology of SP-IR axon and terminals in whole-mount atria

Similar to CGRP-IR axon and terminals in the different regions of the left and right atria, we found that several large SP-IR axon bundles entered the atria and bifurcated into smaller bundles (Figure 12). Axons, terminal end-nets and free endings were seen in all regions (e.g., Figure 12D and12E). In addition, varicose endings around PNs were also seen (Figure 12F). Compared to CGRP-IR axon and terminals, we found that there were much less SP-IR axons and terminals. Therefore, we did not present the montage of the whole atria to show the overall innervation and distribution of SP-IR axons and terminals.

CGRP-IR and SP-IR innervation: dual labeling in the atria

Most SP-IR fibers also demonstrated CGRP immunoreactivity (Figure 13). Within cardiac ganglia, the majority of SP-IR varicose terminals in ICGs were also immunoreactive for CGRP (Figure 14), whereas some CGRP-IR varicose terminals (green) did not exhibit colocalization of SP immunoreactivity. In the other areas of the atria including the auricles and the entrance area of the major veins, we also found colocalization of SP and CGRP in axons and terminals (not shown).

Since there were significantly more CGRP-IR axons and terminals than SP-IR axons and terminals, we examined whether the effectiveness or sensitivity of the SP antibody in labeling the axons was comparable to the CGRP antibody. We used immunohistochemistry to label CGRP-IR and SP-IR axon fibers and terminals in the small intestine. We found that CGRP and SP antibodies both strongly labeled axons and detailed terminal structures in the small intestine (Figure 15). CGRP-IR axons innervated the myentric ganglionic plexus and formed extensive varicose endings around individual neurons with few free endings in the circular muscle, if any (Figure 15A and 15D). SP-IR axons terminated in the myentric ganglionic plexus and formed extensive varicose endings around individual neurons as well as extensive networks in the circular muscle layer (Figure 15E). Interestingly, SP-IR axons and terminals barely colocalized with CGRP-IR axons and terminals (Figure 15C).

DISCUSSION

In this study, we have for the first time characterized the distribution and morphology of CGRP-IR and SP-IR axons and terminals in different areas over the whole-mount atria of the FVB mouse model. These CGRP-IR and SP-IR axons presumably originated from the dorsal root ganglia (DRG) (see below discussion), thus they are sympathetic afferent axons. The detailed documentation of the arrangement and structural details of sympathetic afferent axons and terminals in the whole-mount atria may provide a foundation for the future study of pathological remodeling of cardiac sympathetic afferent axons and terminals in diseases models.

Origin of CGRP-IR and SP-IR axons.

The extrinsic origin of cardiac CGRP-IR and SP-IR axons in the atria is an issue that has not yet been resolved. In our study, we have examined all cardiac ganglia. We found 15-20 cardiac ganglia of different sizes on the dorsal surface of the both right and left atria. The cardiac ganglionic principal neurons (PNs) in these ganglia were neither CGRP-IR nor SP-IR, indicating that cardiac CGRP-IR and SP-IR axons were not intrinsic (i.e., from these cardiac ganglia) and thus must be extrinsic (i.e., from DRG or Nodose ganglia). Since both DRG and the nodose ganglia may contain CGRP-IR and SP-IR cardiac sensory neurons in dogs (Hoover et al. 2008), we had assumed that both DRG and the nodose ganglia might have contributed to the CGRP-IR and SP-IR axons and terminals in the mouse atrial tissue. In rats, we previously found that one of the major terminal structures of vagal afferent axons from the nodose ganglion are the

terminal flower-sprays in the atria (Cheng et al. 1997), which has been confirmed in our recent study of vagal afferent projections to the aortic arch (Li et al. 2010) and atria in mice (unpublished). Therefore, we believe that the CGRP-IR and SP-IR cardiac axons are most likely from the DRG, rather than from the nodose ganglia. This is further supported by Hoover et al (2008) who injected the tracer HRP to the heart to label cardiac sensory neurons in the DRG and nodose ganglia, and then stained for CGRP-IR and SP-IR neurons. They found that HRP-labeled DRG neurons were 21% CGRP-IR, 13% SP-IR, and 6% CGRP/SP-IR. In contrast, HRP-labeled neurons in nodose ganglia were neither CGRP-IR nor SP-IR.

Innervation, distribution and morphology of CGRP-IR and SP-IR axons and terminals in the whole-mount atria of mice.

In sliced preparations, previous studies demonstrated the CGRP-IR and SP-IR axon innervate the atria in different species (Saito A et al., 1986; Parsons and Neel, 1987; Papka and Urban, 1987; Shoba and Tay, 2000; Pan and Chen, 2002; Richardson et al., 2003; Hoover et al., 2008, 2009; Mousa et al., 2010). Since tissue cutting may damage the 3-D structures of the axons and terminals, these studies could not show the complete distribution and morphology of the axons and terminals over the entire atrium. Although some studies labeled CGRP-IR and SP-IR axons and terminals in the whole-mount cardiac tissue, the focus was mainly on innervation of cardiac ganglia (Richardson et al., 2003; Parsons et al., 2006). In contrast to these studies, our study presents a holistic view of CGRP-IR and SP-IR axon distribution, as well as

differentiated terminal structures at different regions of the whole right and left atria (including auricles, the entrance areas of the major veins and cardiac ganglia). In addition, our work demonstrated that CGRP-IR and SP-IR are colocalized in the terminals within cardiac ganglia and formed pericellular endings around PNs as well as varicose axons coursing through cardiac ganglia, whereas R. J. Richardson et al. only found CGRP-IR and SP-IR varicose axons which did not form pericellular endings around cardiac PNs in rats. Our study shows for the first time the complete innervation, distribution, and morphology of sympathetic (spinal) afferent axons and terminals in the mouse atria. No comparable studies have been found.

Functional implications

The sympathetic afferent neurons in the DRG are unipolar neurons. The central limb of cardiac sympathetic afferent axons ends in the dorsal horn of the spinal cord and the peripheral limb projects to the heart. Many studies have demonstrated that CGRP and SP are localized in the axons and terminals centrally and peripherally (Willis and Coggeshall, 1991; Seybold, 2009). Centrally, CGRP-IR and SP-IR terminals innervate the neurons in the dorsal horn to transduce pain sensations. Peripherally, CGRP-IR and SP-IR terminals are nociceptive sensory receptors. In our study, we examined peripheral sympathetic afferent innervation in the atria. We found that CGRP and SP-IR axons and terminals are in the epicardium, myocardium and intrinsic cardiac ganglia. One important issue is why the sensory nerve terminals (which are supposed to be sensory receptors) contain CGRP and SP, which are both neurotransmitters. This is

unusual because neurotransmitters should be in the presynaptic vesicles of motor axon terminals, and not in sensory nerve terminals. In cardiac ganglia, physiological and pharmacological studies have demonstrated that application of SP directly to cardiac ganglionic cells may depolarize the membrane potentials, thus enhancing parasympathetic efferent control of cardiac ganglia (Hoover et al., 2000; Figure 16). As to whether CGRP may have any direct effects on cardiac ganglionic neurons is still an issue (which is the question mark in Figure 16). Anatomically, there are many CGRP-IR axons and terminals around cardiac ganglionic neurons (PNs) as shown in our present study. However, the evidence for the direct physiological effect of CGRP on PNs is still absent. Several groups applied CGRP to cardiac ganglia and made intracellular recordings of the activity of PNs in an attempt to examine the effect of CGRP on PNs physiologic properties, but they failed to find any positive effects (personal communications). Since our anatomical data clearly demonstrated that CGRP-IR axons formed many synaptic varicose contacts with PNs, we postulate that such a connection of CGRP-IR axons with PNs may have functional implications which should be examined in the future. In our preparation, we found many more CRGP-IR than SP-IR axons and terminal in atrial muscles. Consistent with such a finding, Hoover et al. observed abundant CGRP receptors but less SP receptors in atrial muscles (Hoover and Hancock, 1988; Chang et al., 2001). Presumably, CGRP and SP may regulate heart rate, AV conduction and cardiac contractility (Hoover et al., 2000; review). In the entrance area of major veins to the atria, we found CGRP-IR and SP-IR axons and terminals, which is consistent with the finding that CGRP and SP may have a

vasodilatory effect. Recently, it has been shown that CGRP and SP are released by activation of TRPV1 receptors during cardiac ischemia, which increases preconditioning and plays an important protective role during cardiac ischemia (Bolli and Abdel-Latif, 2005; Wang and Wang, 2005; Li et al., 2008; Zhong and Wang, 2008).

Technical considerations.

In this study, we found that there were many more CGRP-IR axons and terminals than SP –IR axons and terminals. One concern was whether our immunostaining protocol was sensitive enough to label SP-IR axons and terminals in the atria. To test whether our protocol could effectively label the SP-IR axons and terminals, we used the small intestine as a control. The SP antibody could effectively label SP-IR axons and terminal networks in the circular muscle layer and pericellular endings around myenteric ganglionic neurons in the small intestine. We also labeled CGRP-IR axons and terminals in the small intestine. Compared to CGRP-IR axons and terminals, there are many more SP-IR axons and terminals than CGRP-IR axons and terminals in the circular muscles. This implies that our protocol can effectively label SP-IR axons and terminals in the muscular layer. Therefore, we believe that there are indeed more CGRP-IR axons and terminals than SP-IR axons and terminals in the atrial muscles.

In this study, we only performed CGRP and SP immunoreactivity in whole-mount atria. Since the ventricle wall is much thicker than the atrial wall, it is questionable whether our protocol may be directly applied to the ventricles due to potential penetration problems. In the future, we need to improve our methods for ventricular

dissection, immunohistochemistry, and/or adopt our approach to use direct injection of fluorescent tracers into the DRG to label sympathetic afferent axons and terminals in the ventricles.

PERSPECTIVES

In this study, we have presented a detailed documentation of the innervation, distribution and morphology of CGRP-IR and SP-IR axons in the whole-mount atria of mice. It has been shown that diseases (such as aging, sleep apnea, diabetes, and cardiac failure) may remodel the autonomic nervous system. Previously, we examined the effects of aging, intermittent hypoxia and diabetes on the vagal afferent and efferent innervation of the atria and aortic arch (Ai et al. 2007; Lin et al. 2008; Li et al. 2010). Schmidt et al. (2008) examined the aging and diabetes-induced changes of sympathetic postganglionic neurons and efferent axons. Presumably, these diseases may also damage the sympathetic afferent nerves as well. Previously, it has been assumed that sensory nerve degeneration may lead to silent cardiac ischemia in diabetic patients (Faerman et al., 1977; Gutterman, 2009). Recently, studies have shown that diabetes may reduce TRPV1, CGRP, and SP mRNA expression which may impair the post-ischemic recovery in the hearts of diabetic mice (Song et al 2009; Wei et al. 2009). Our study has provided a foundation for the future qualitative and quantitative analysis of the pathological changes of sympathetic cardiac afferent axons and terminals in mouse models, which may shed the light on the neural mechanisms for painless cardiac ischemia as well as for the reduced beneficial effects of preconditioning against ischemia/reperfusion-induced heart injury.

APPENDIX: TABLES AND FIGURES

Table 1: Antibodies Used

Antibody	Concentration	Host	Company	Emission
Anti-CGRP†	1 µl/ml	Goat	Abcam	n/a
Anti-SP†	2 µl/ml	Rabbit	Immunostar	n/a
Anti-Goat††	24 µl/ml	Donkey	Invitrogen	594 nm
Anti-Rabbit††	24 µl/ml	Donkey	Invitrogen	660 nm*

†primary
††secondary
*infrared fluorophores are invisible to human eyes

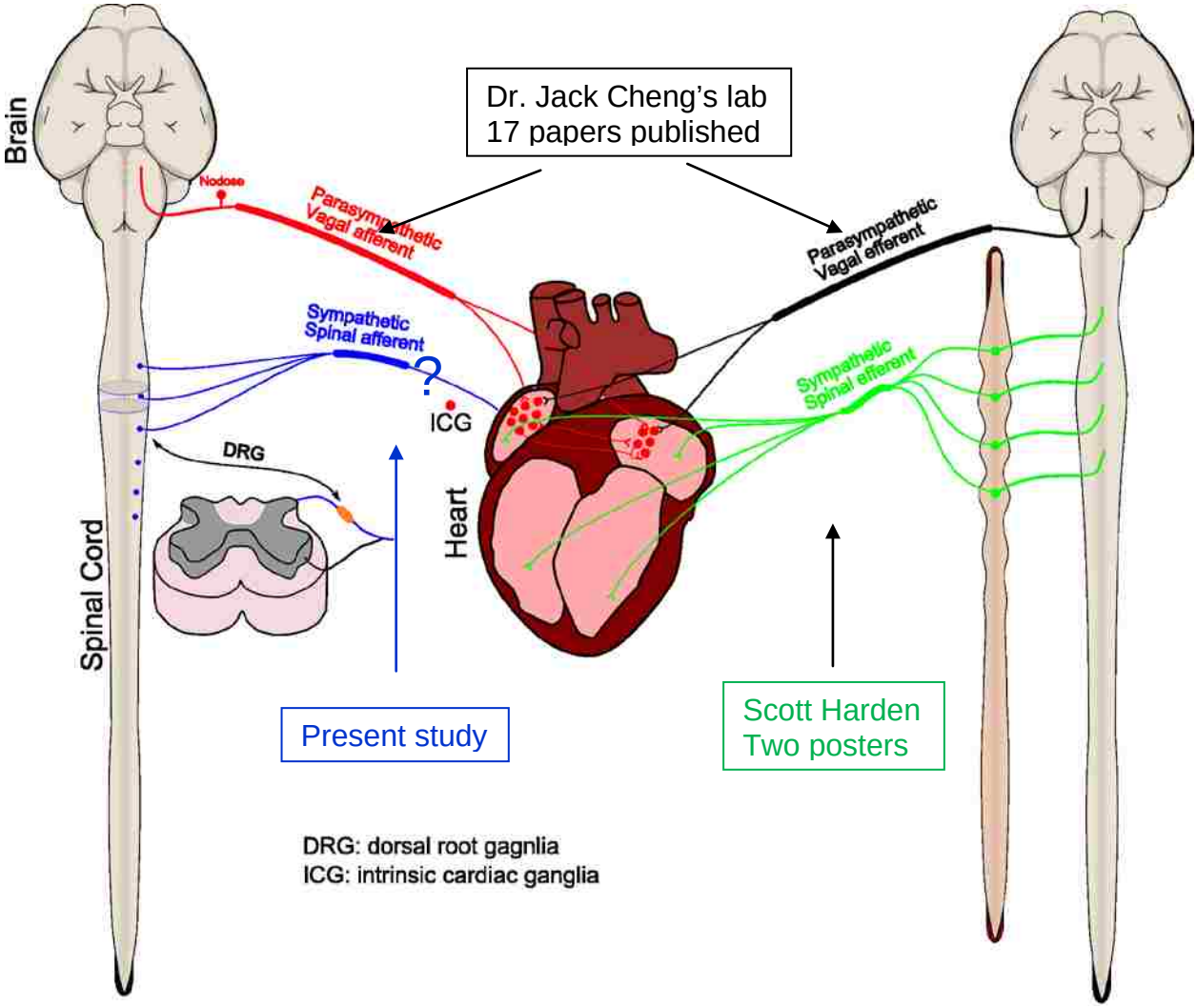

Figure 1. Autonomic nervus system research progress review

A schematic drawing shows the summary of the research projects in Dr. Jack Cheng's lab. 17 papers related to the parasympathetic afferent and efferent pathways have been published. In addition, two posters related to cardiac sympathetic efferent pathways have been presented in the international scientific meetings (Scott et al. 2009; 2010). The focus of the present study is to examine the innervation, distribution, and morphology of sympathetic (spinal) afferent axons and terminals in the atrium.

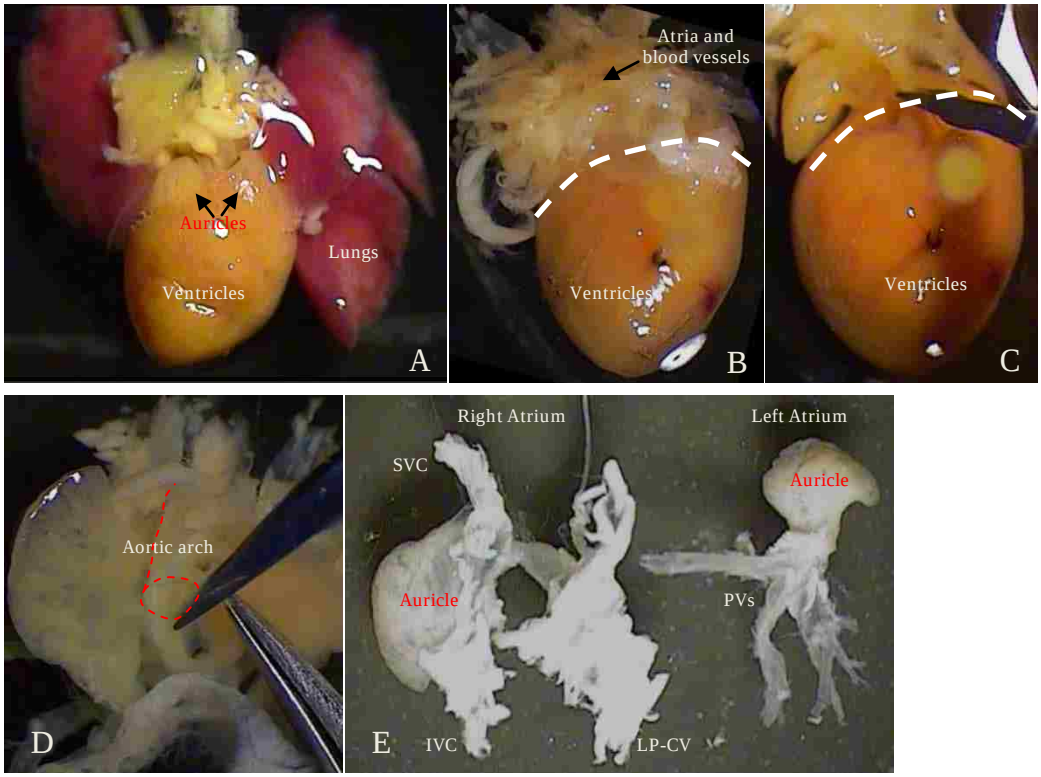

Figure 2 Tissue preparation.

A. Heart and lungs were removed from a perfused and post-fixed FVB mouse.

B. Atrium and ventricles from the FVB mouse – esophagus, lungs and trachea were removed.

C. Atria were separated from the ventricles by cutting along the interatrial-ventricular groove.

D. The aortic arch was separated from the atria and pulmonary artery was removed.

E. Right and left atrium were separated by cutting along the interatrial septum.

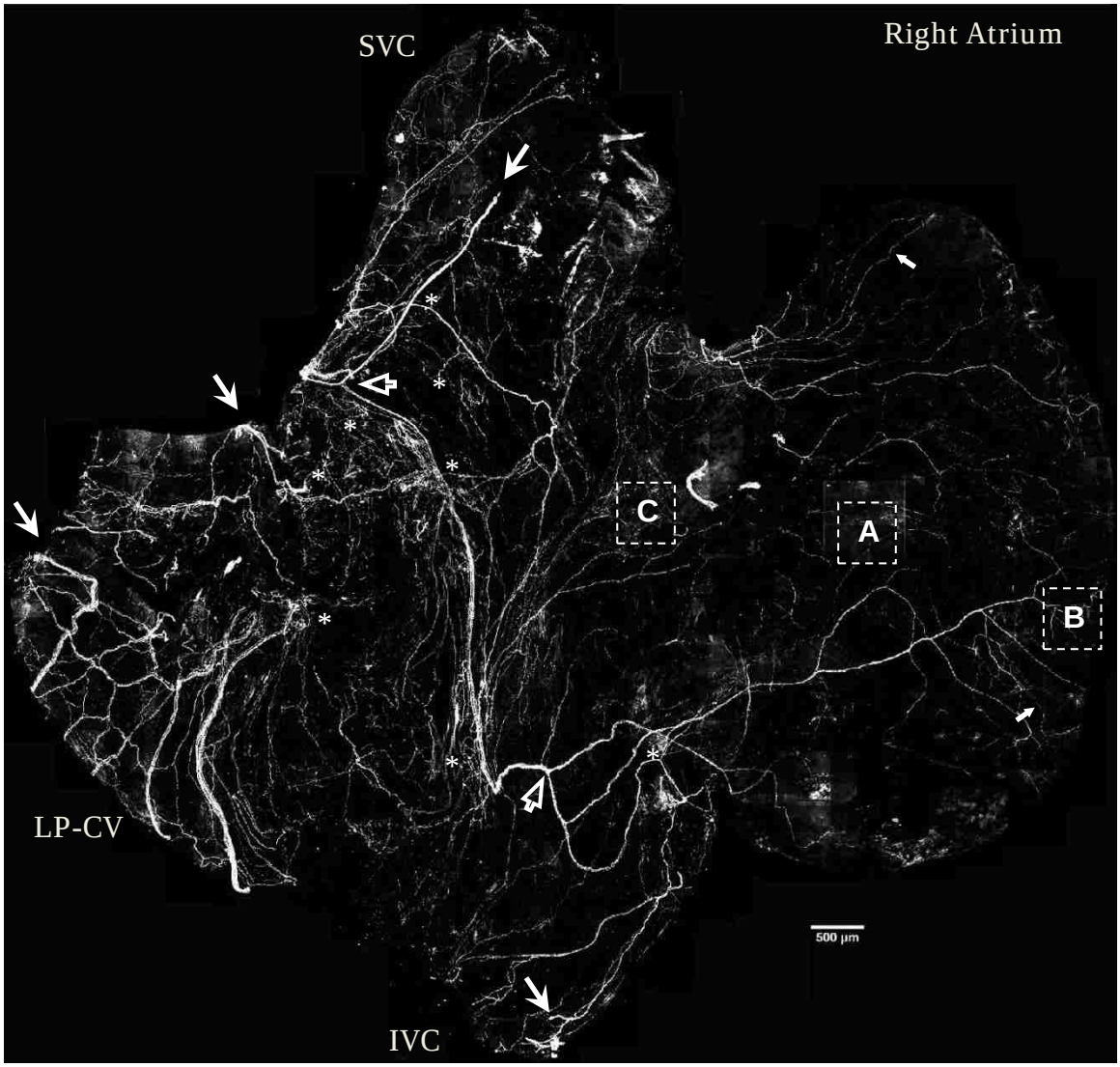

Figure.3 A montage of all-in-focus maximum confocal projections showing CGRP-IR innervation and distribution in the right atrium of a FVB mouse.

A few large CGRP-IR axon bundles (indicated by solid arrows) entered the right atrium from SVC and L P-C V. Then, they bifurcated into small bundles (indicated by open arrows) and single axons (indicated by small arrows). Finally, these single axons covered all regions with terminal networks (see Figures 5 and 6 for detail) of the atrium, including the auricle and the entrance area of IVC, SVC and L P-C V. In addition, CGRP-IR axons innervated multiple ICGs with varicose endings around individual cardiac ganglionic principal neurons as indicated by * (see Figures. 5 and 7 for detail). Inferior vena cava: IVC;

superior vena cava: SVC; left precaval vein: L P-C V. Intrinsic cardiac ganglion: ICG. Scale bar: 500 μm. Note: Since this is a confocal montage which shows the overall distribution of CGRP-IR axons, the detail structures of the axons and terminals are not visible in this image. The dotted frames A, B, and C are the sampling windows where the detail structure of axon terminals will be presented in Figure 6.


B
A
C
PV
PV
PV
PV
PV
500 µm
Left Atrium

Figure 4. A montage of all-in-focus maximum confocal projections showing CGRP-IR innervation and distribution of the left atrium of a FVB mouse.

A few large CGRP-IR axon bundles (indicated by solid arrows) entered the left atrium from left and right PVs. Then, they bifurcated into small bundles (indicated by open arrows) and single axons (indicated by small arrows). Finally, these single axons covered all regions with terminal networks (see Figures 5 and 6 for detail) of the atrium, including the auricle and the entrance area of PVs. In addition, CGRP-IR axons innervated multiple ICGs with varicose endings around individual cardiac ganglionic principal neurons as indicated by * (see Figures 5 and 7 for detail). Pulmonary veins: PVs. Scale bar: 500 μm. Note: Since this is a confocal montage which shows the overall distribution of CGRP-IR axons, the detail structures of the axons and terminals may not be visible in this image. The dotted frames A, B, and C are the sampling windows where the detail structure of axon terminals will be presented in Figure 6.

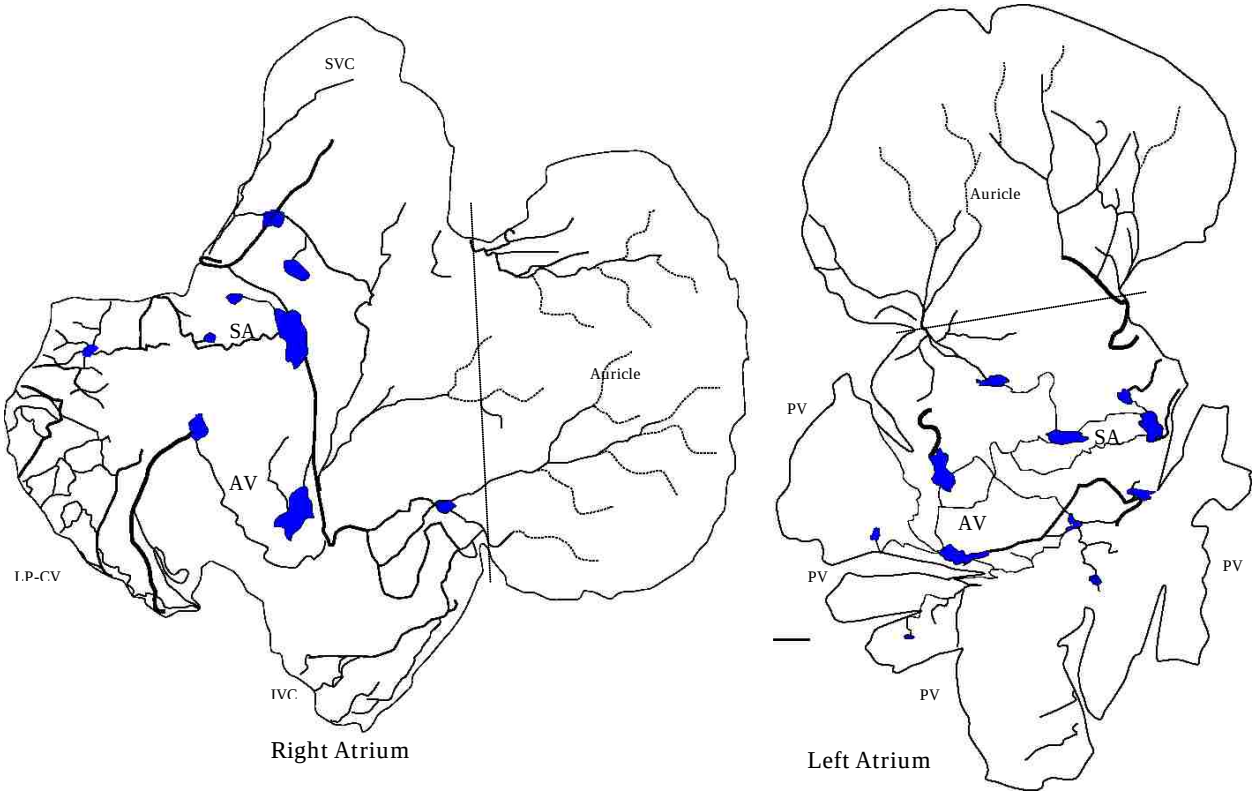

Figure 5. Two schematic drawings showing innervation and distribution of CGRP-IR axons in the whole-mount right and left atria in the FVB mouse as shown in Figures 3 and 4.

Each atrium was divided into an auricle region and the rest of the atrium including the entrance of the large veins. The boundary is indicated by a dotted straight line. Large bundles of CGRP-IR axons (thick lines) entered the atrium and then bifurcated into small bundles (thin lines) and ultimately the single axons (dotted lines) with terminal networks and free endings (not shown at this magnification). Both atria contained multiple intrinsic cardiac ganglia as indicated by blue blobs. SA, sino-atrial node region; AV atrio-ventricular node region; inferior vena cava: IVC; superior vena cava: SVC; left precaval vein: L P-C V; pulmonary veins: PVs. Scale bar: 500µm.

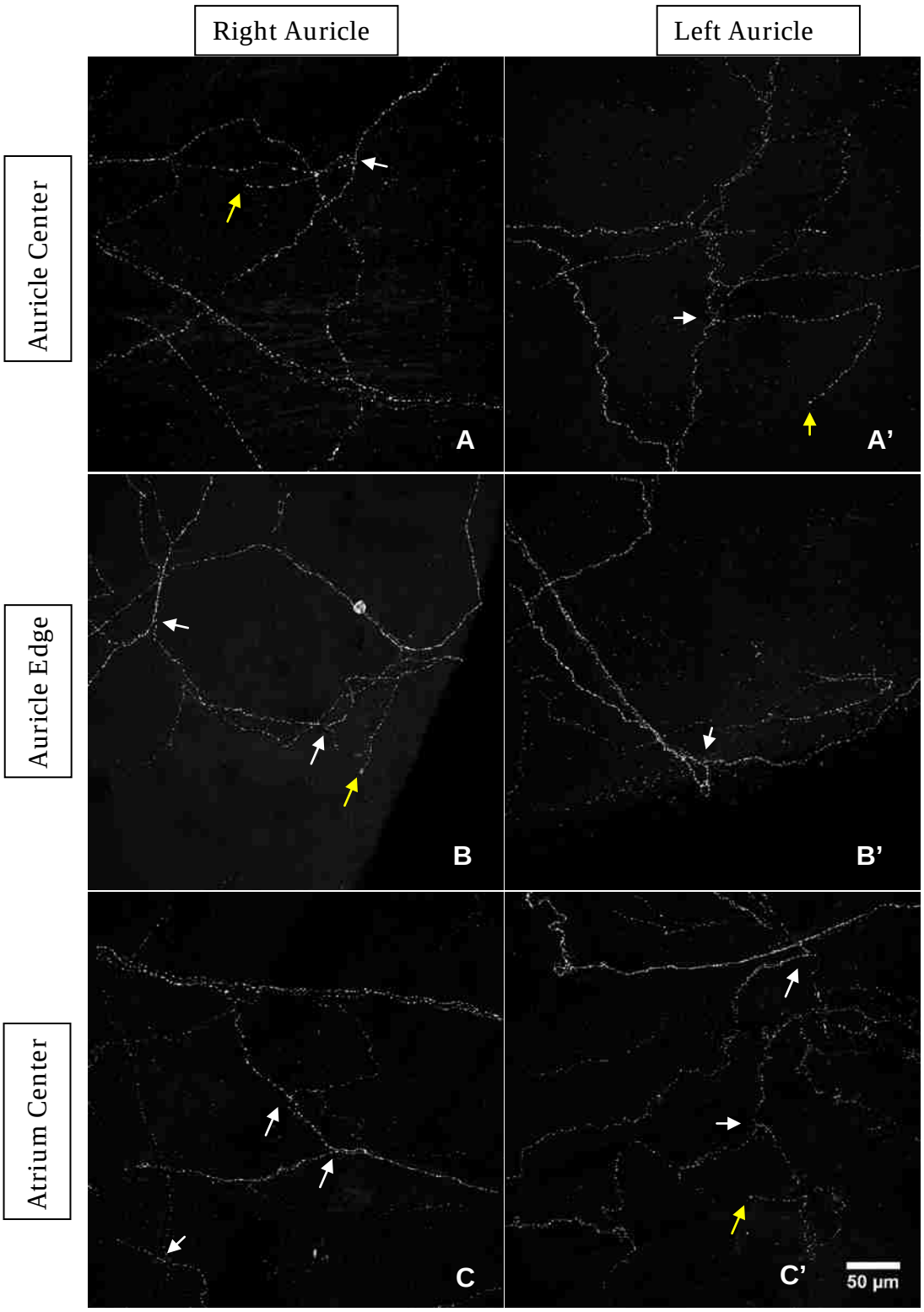
Right Auricle
Left Auricle
Auricle Center
Auricle Edge
Atrium Center
A
A'
B
B'
C
C'
50 µm

Figure 6. CGRP-IR axons and terminals in the atria.

All-in-focus projections at the regions as indicated by A, B, C in the right and left atria in Figures 3 and 4. Detail structures of CGRP-IR axons in different atria regions showed similar patterns. Multiple single axon fibers formed terminal end-nets with free endings in epicardium and myocardium. White arrows: branching points; yellow arrows: free endings. Scale bar: 50μm.

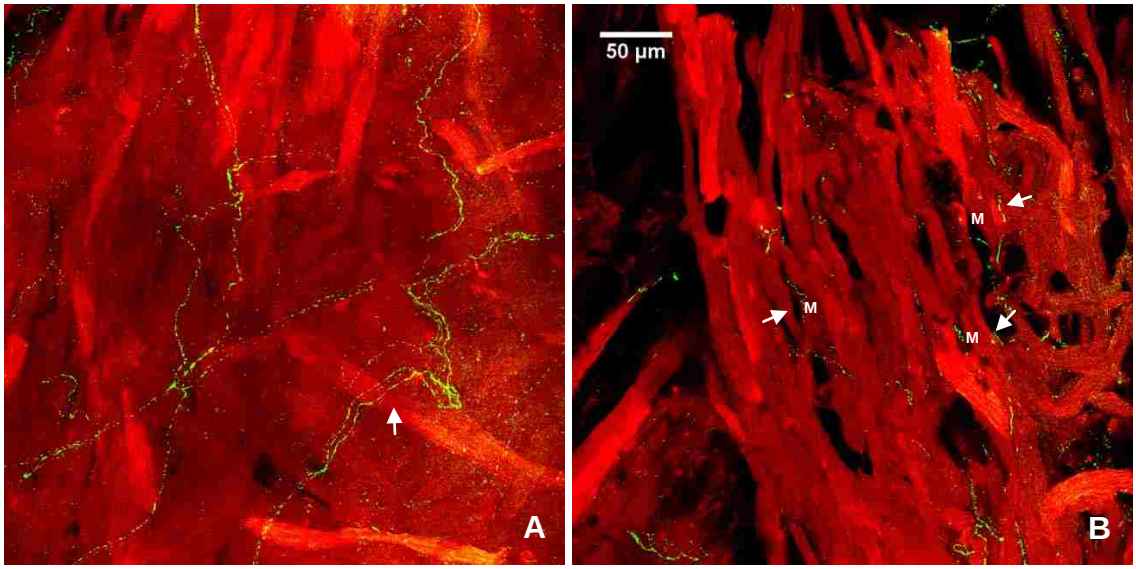

Figure 7. CGRP-IR axons in epicardium and myocardium.

A. A partial projection confocal image showing several axons (arrow) traveling in the epicardium (on the surface of cardiac muscle). B. A single optical section showing that delicate CGRP axons (arrows) are in myocardium and have close contacts with myocytes. M. cardiomyocytes. Scale bar: 50μm.

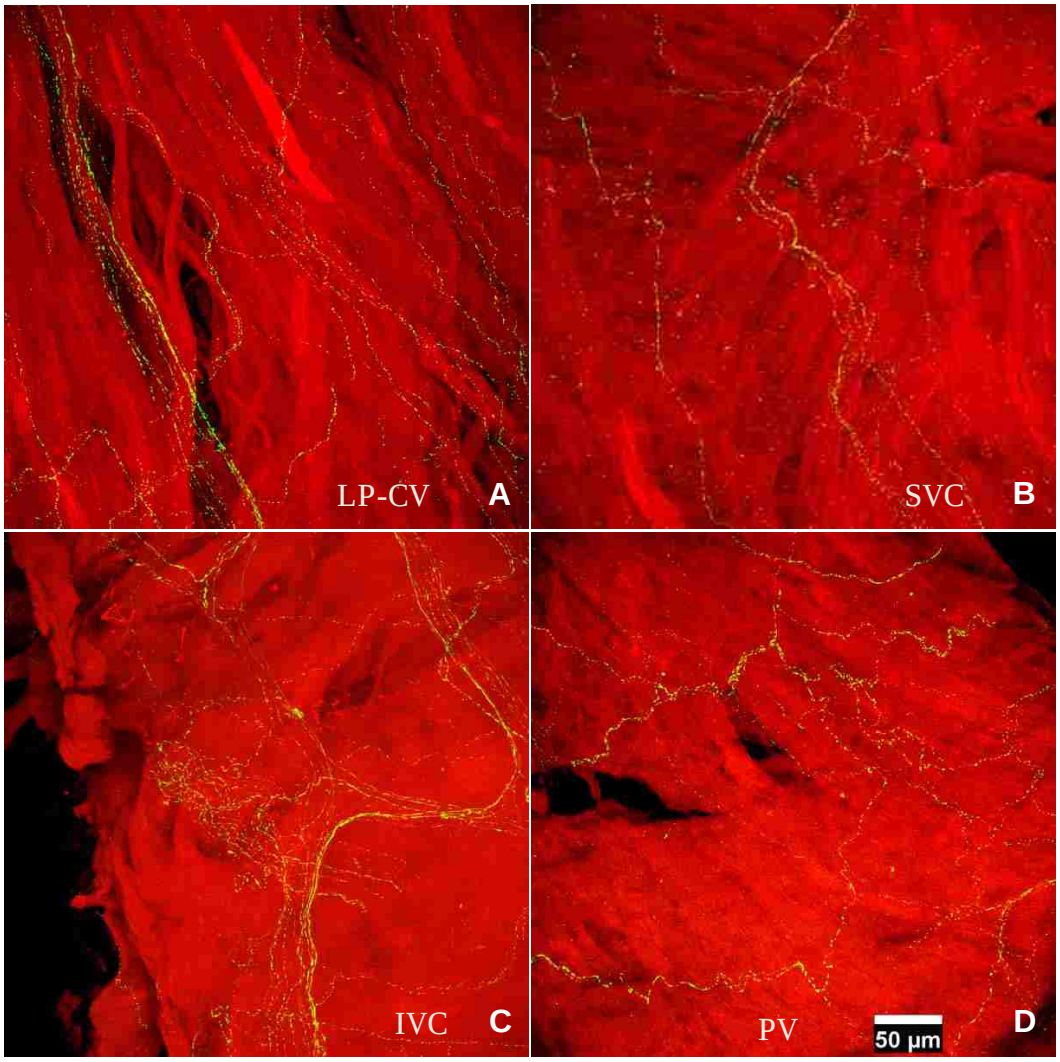

Figure 8. CGRP-IR axons in the entrance area of the major veins.

All-in-focus projection images in: LP-CV (left precaval vein), SVC (superior vena cava), IVC (inferior vena cava) of the right atrium; and PV (pulmonary vein) of the left atrium. Green color represents CGRP-IR axons and red color represents autofluorescent background from atrial muscle layers (M). CGRP-IR axons innervated the smooth muscles in atria exhibit the similar structure of terminal end-nets and free endings as seen in the rest of the atria. Scale bar: 50 µm.

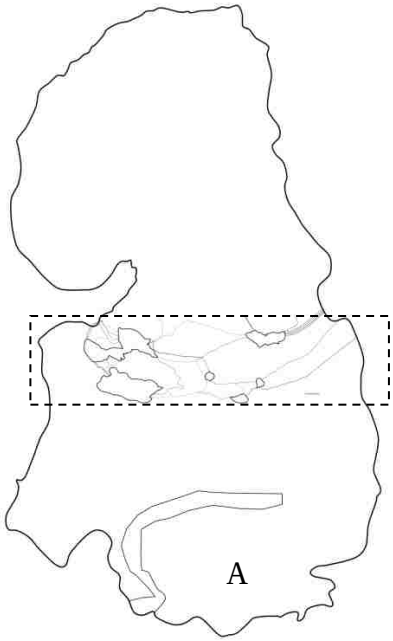
A

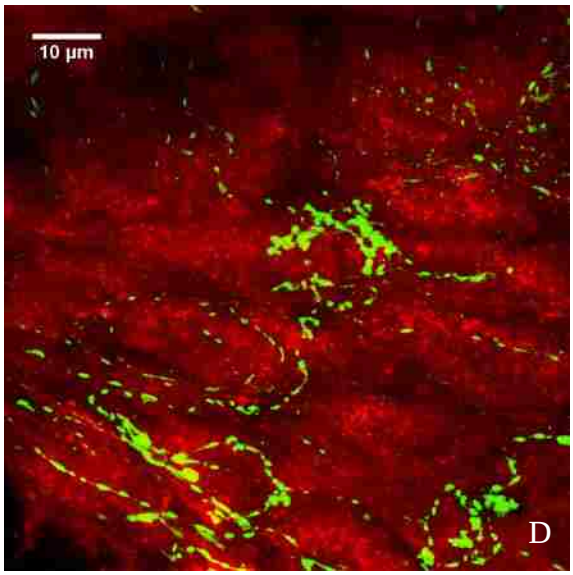
10 µm
D

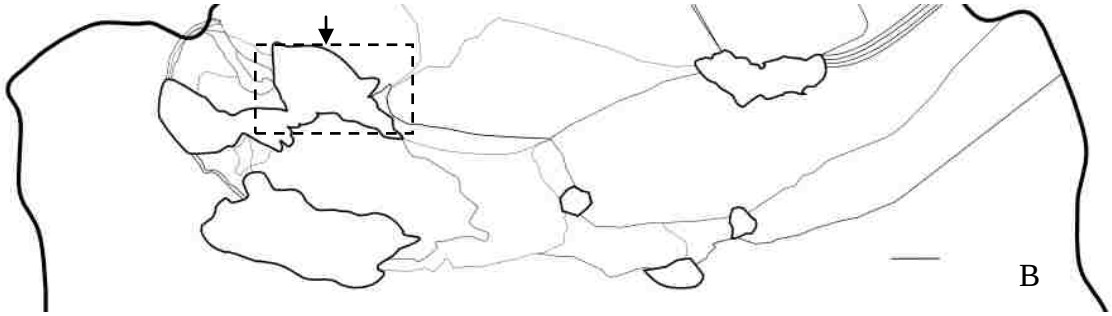
B

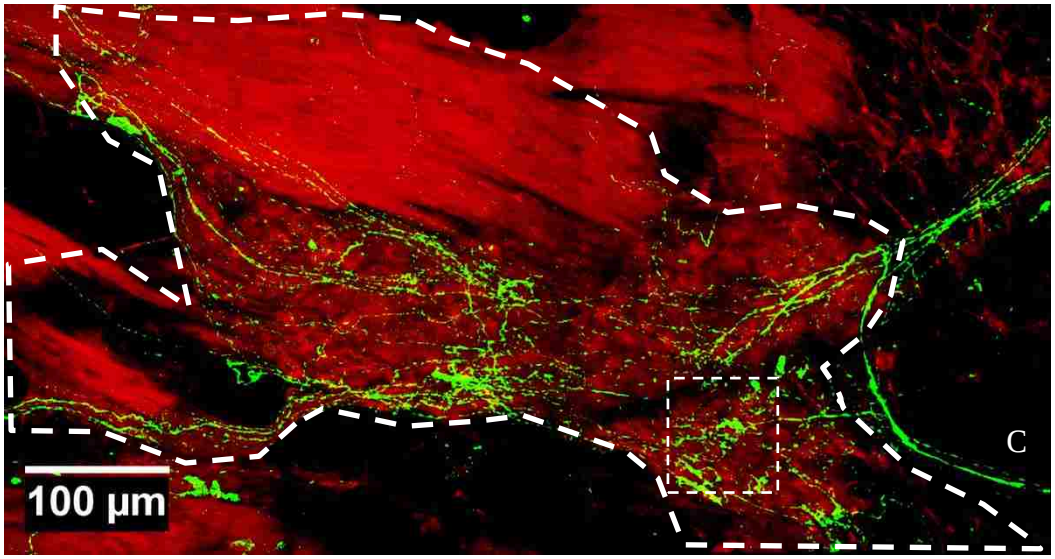
100 µm
C

Figure 9. CGRP-IR axons innervation of intrinsic cardiac ganglia (ICGs) in the left atrium of a representative mouse.

A. Schematic drawing of the left atrium. In the dotted region, CGRP-IR axons (Green color) innervated ICG neurons (Red color, autofluorescence). B. The dotted region in panel A at high magnification. C. A partial projection of confocal optical sections from the ganglion (indicated by an arrow) in panel B showing that CGRP-IR axon traveled in the connectives between ICGs. Some of these axons passed by the ganglia, whereas others formed axonal varicosities around cardiac ganglionic principal neurons (PNs). D. A High magnification of the boxed area in C showing such axonal varicosities around PNs. Noticeably, none of PNs were CGRP-IR. Scale bar: 200 μm in panel A and panel B; 100 μm in panel C.; 10 μm in panel D.

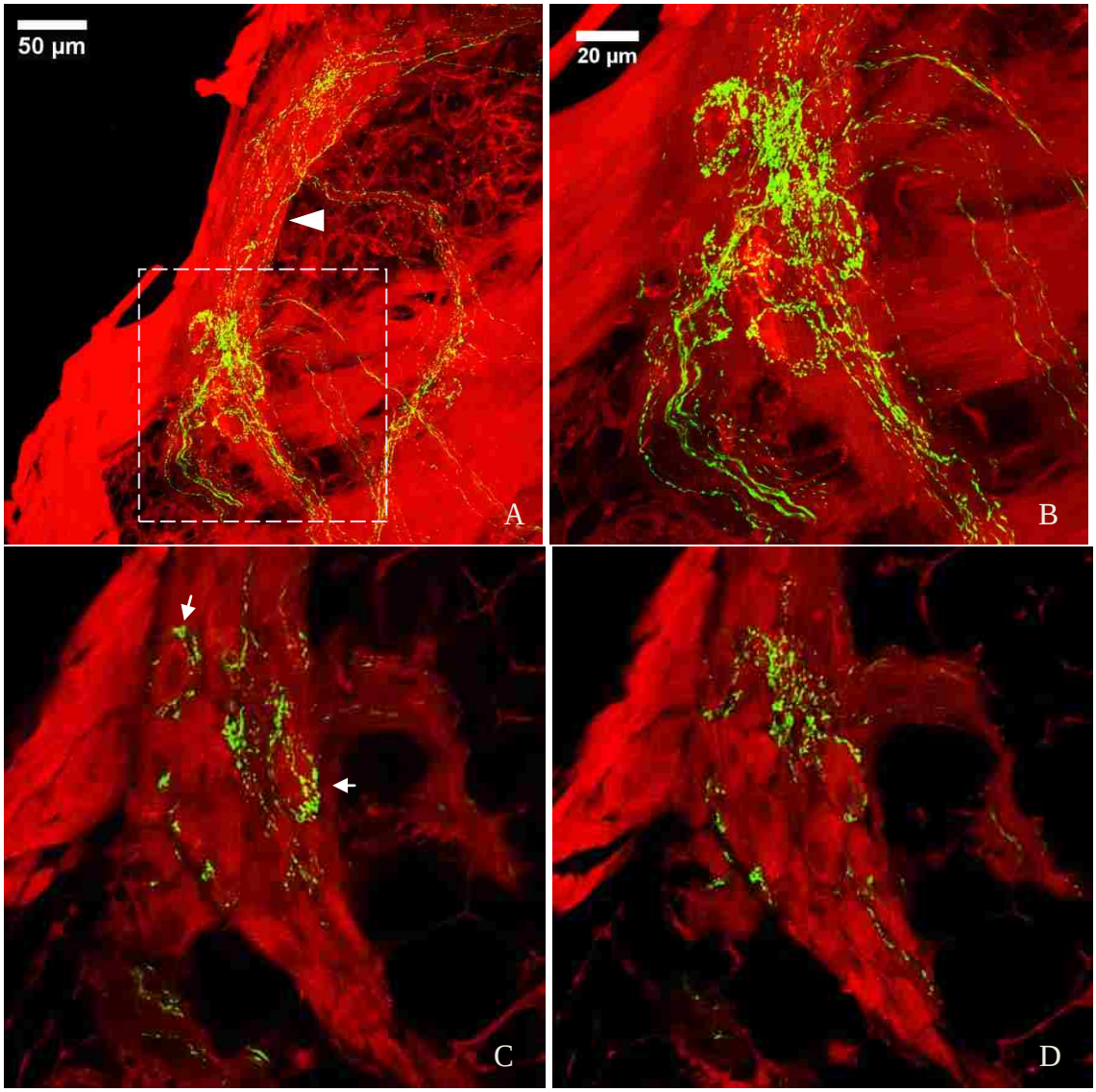

Figure 10. CGRP-IR axon innervation in the intrinsic cardiac ganglia (ICGs) of the right atrium.

A. All-in-focus projection image at the AV region of the right atrium. A ganglion is identified within the dotted frame. B. High magnification of the region with the dotted frame in panel A. C-D. Two different optical sections showing that CGRP-IR varicosities wrapped around the individual PNs (arrows). Triangles indicate CGRP-IR axons are passing by ICG PNs. Green: CGRP-IR; Red: autofluorescence. Scale bars: 50 µm in panel A; 20 µm in panel B-D.

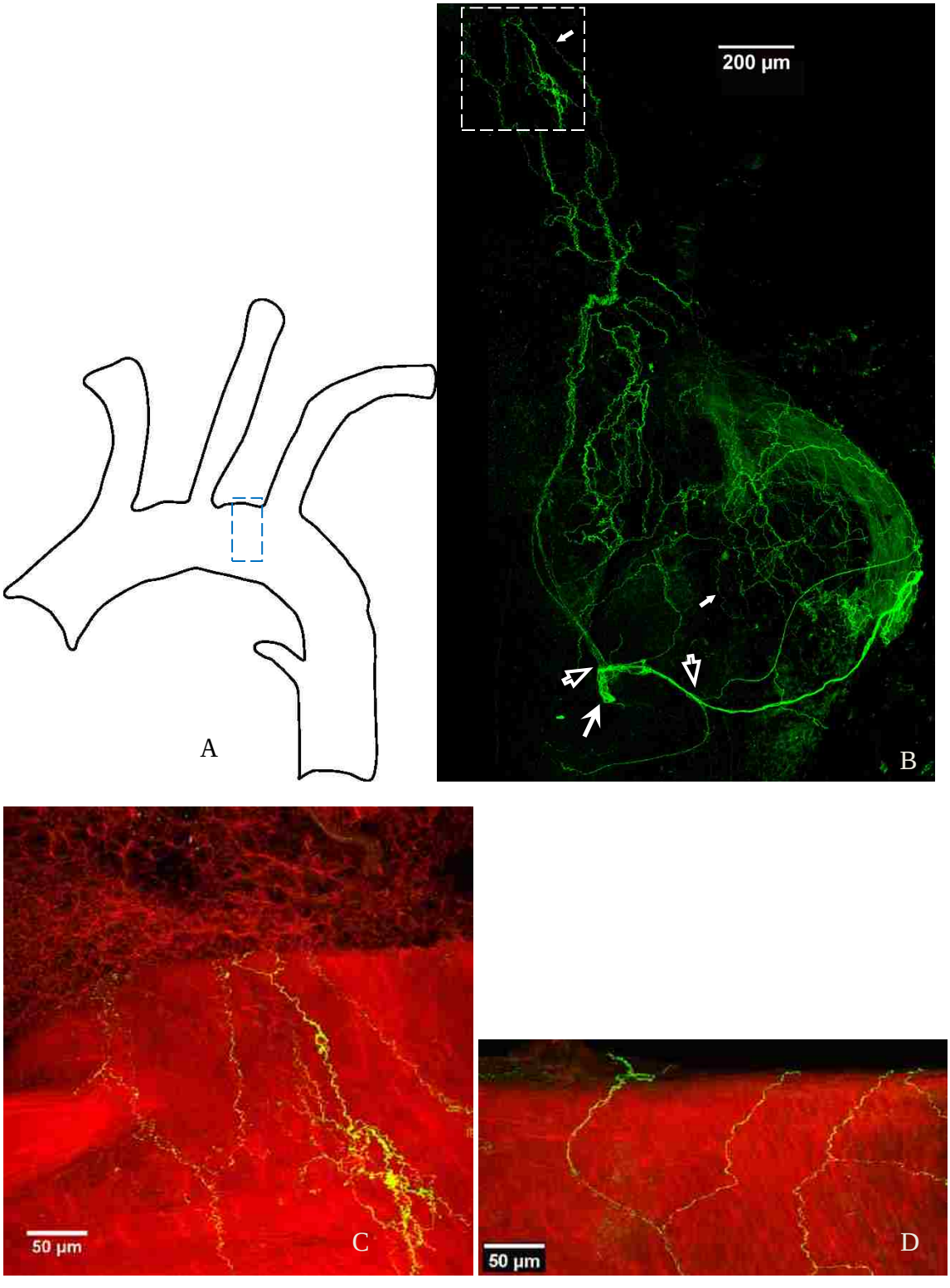
200 µm
A
B
50 µm
C
50 µm
D

Figure 11. CGRP-IR axons in the aortic arch.

A. A schematic drawing of an aortic arch. B. All-in-focus projection confocal montage showing a large CGRP-IR bundle (solid arrow) from the area enclosed by the dotted frame in panel A bifurcated (open arrows) into single axons (small arrow) and formed complex terminal networks on the surface of the aortic arch. C. All-in-focus projection confocal image showing the detail CGRP-IR terminals from the region enclosed by the dotted frame in panel B. D. All-in-focus projection confocal image showing CGRP-IR axons wrapped around the aortic arch. Green: CGRP-IR; Red: autofluorescence of the aortic arch. Scale bar: 200 μm in panel B; 50 μm in panel C and panel D.

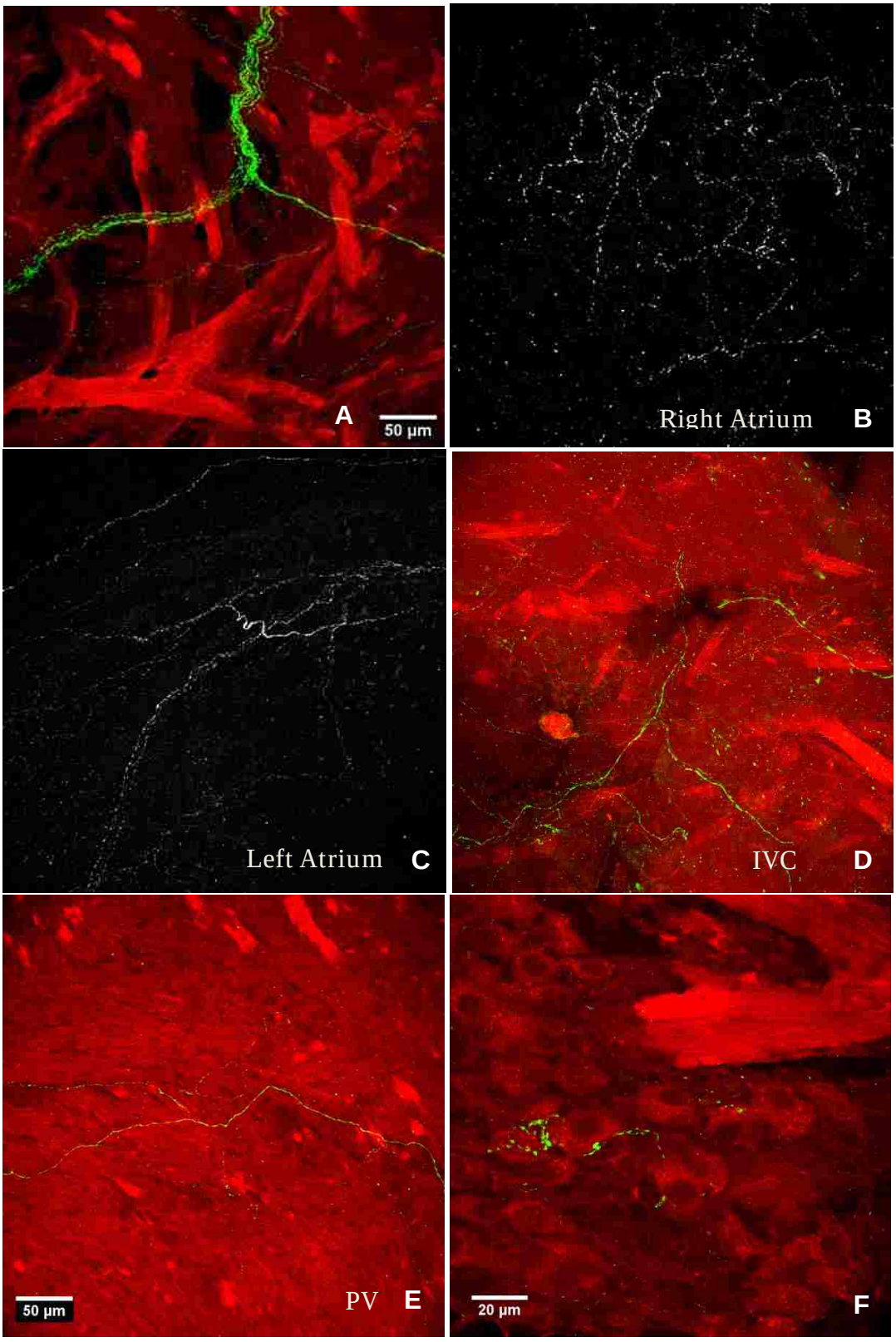
A
50 µm
Right Atrium
B
Left Atrium
C
IVC
D
50 µm
PV
E
20 µm
F

Figure 12 SP-IR axons innervation in atria.

A. A SP-IR axon bundle in the right atrium. B. A SP-IR terminal end-net in the right atrium. C. A SP-IR terminal end-net in the left atrium. D. SP-IR axons in the IVC. E. SP-IR axons in the PV. F. SP-IR axons formed varicose endings around an ICG PN. Scale bars: A-E, 50μm; F, 20 μm.

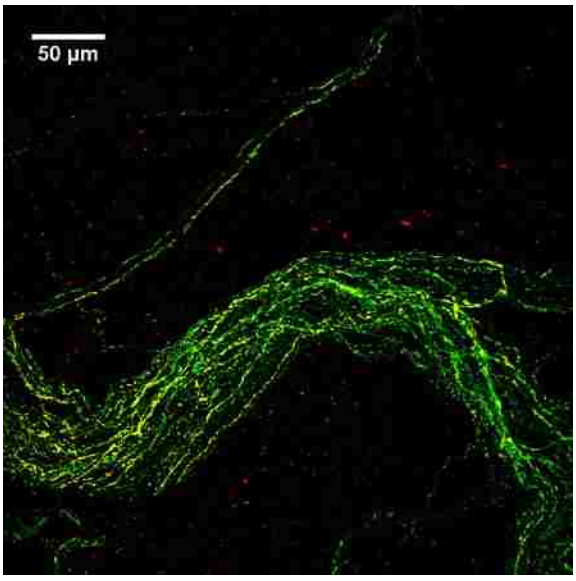

Figure 13 Colocalization of SP-IR axons with CGRP-IR axons in an axon bundle.

A large axon bundle entered the right atrium and most SP-IR (Red) fibers were found to have colocalized with CGRP-IR (Green) fibers, indicating coexpression of CGRP with SP (Yellow) in most SP-IR fibers.

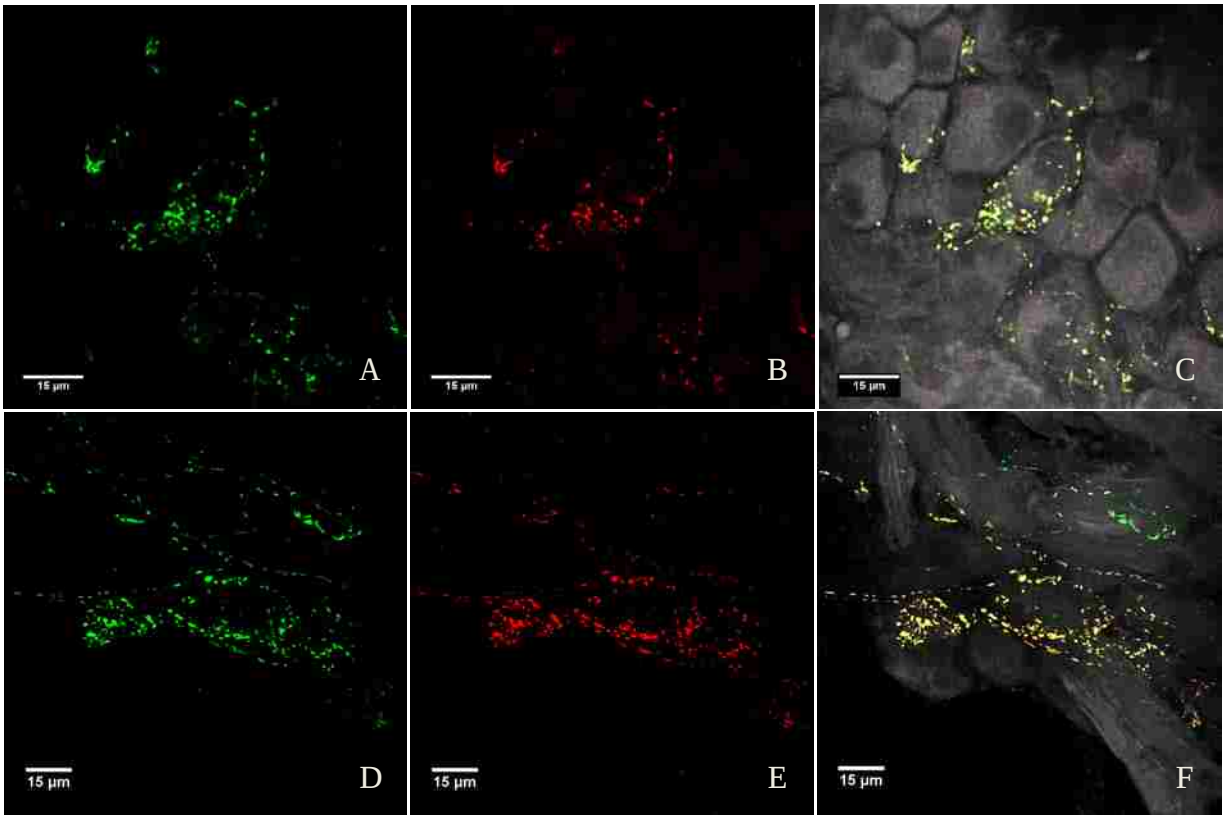

Figure 14. CGRP-IR and SP-IR Innervation of the ICGs: dual labeling.

A. Single confocal optic image shows CGRP-IR terminal varicosities. B. Single confocal optic image shows SP-IR terminal varicosites. C. The merged image of panel A and panel B. PNs are in gray color. Most of the SP-IR varicose terminals show colocalization of CGRP-IR in their terminal varicosities. Colocalization of SP (Red) and CGRP (Green) in these terminals is signified by yellow in the composite image (Red + Green) . Varicosities in pure green (CGRP-IR) color in panel C and panel F suggests that although most SP-IR fibers show colocalized CGRP expression (Yellow), there are also many fibers showing exclusive CGRP immunoreactivity (Green).

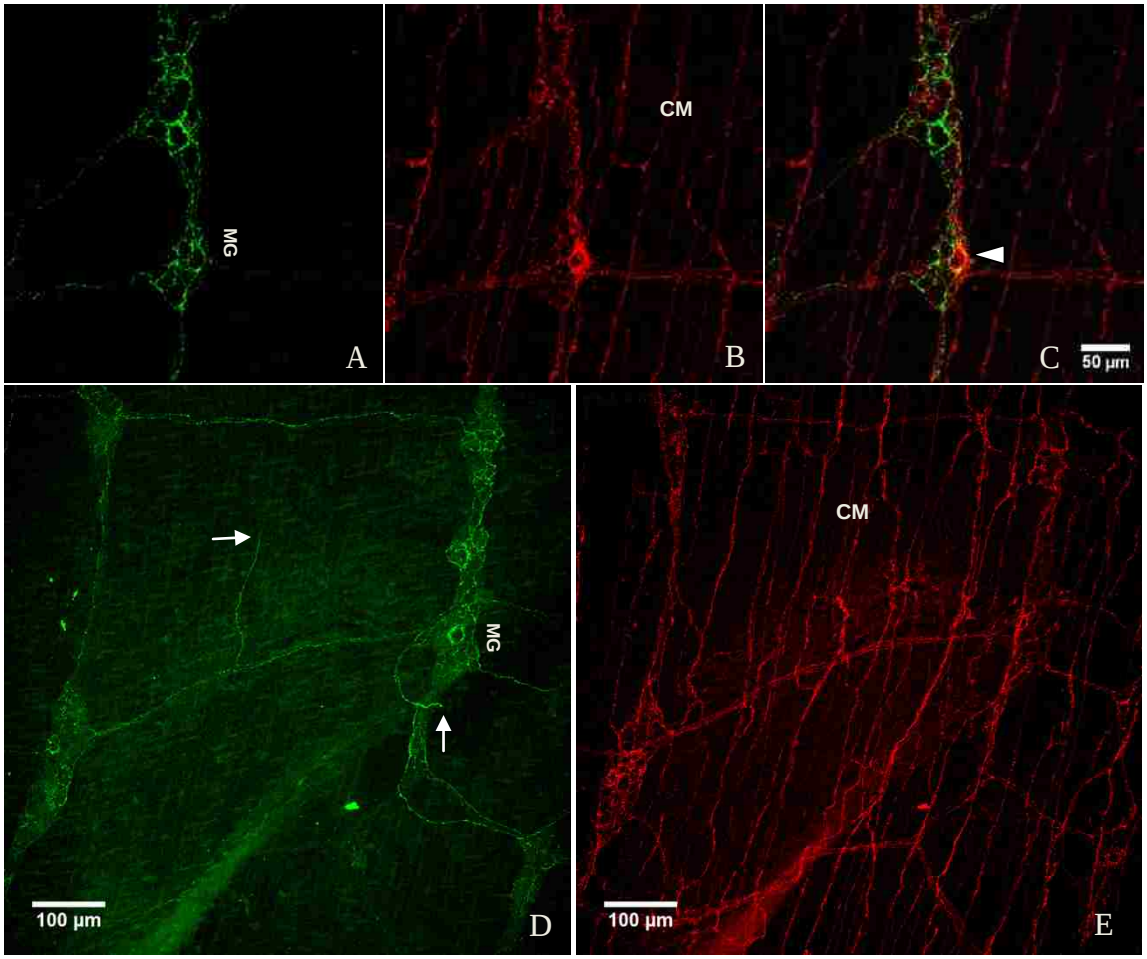

Figure 15. CGRP-IR and SP-IR axons and terminals in the small intestine of a FVB mouse.

A, B. Single confocal optic sectioned images show CGRP-IR (panel A), SP-IR (panel B) fibers and terminals in the small intestine. C. Only a few varicosities show colocalized CGRP-IR and SP-IR as yellow (trangle) in the composite images, whereas the majority do not. D E. All-in-focus projection confocal images show CGRP-IR axons are mostly in the myenteric ganglia and only a few are in the muscle layer (arrows), whereas many SP-IR axons are found richly both in circular muscles and myenteric ganglia . Arrows: Free terminals. CM: Circular muscle. MG: Myenteric ganglia. Green: CGRP-IR; Red SP-IR; Yellow; CGRP-IR + SP-IR.

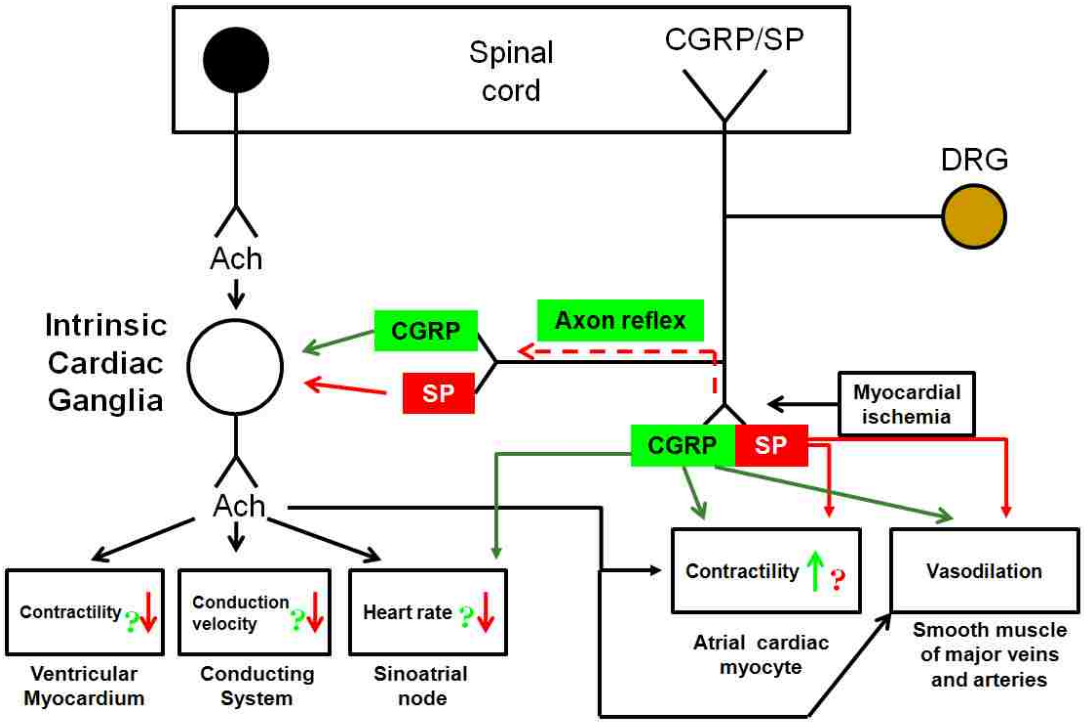

Figure 16. Summary diagram of CGRP and SP innervation and functions in the atria

CGRP-IR and SP-IR axons innervate ICGs, atrial myocytes and blood vessels. During insults (e.g., ischemia), CGRP-IR and SP-IR axon terminals are activated by endogenous chemicals (e.g. bradykinin) which are released from the injured cardiac tissues and these pain signals are then sent to the central nervous system (the spinal cord). In the meantime, CGRP-IR and SP-IR axon terminals may also have "motor" functions, i.e., CGRP and SP may be released at these axon terminals locally to regulate the SA heart rate, AV conduction, atrial muscle contractility, and vasodilation. These neuropeptides are either released from the same axonal terminals or through the axon reflex mechanism (i.e., the chemical simulation is at one site and the action is at another site nearby). ? indicates that the effects of CGRP-IR axons on the target have not been completely elucidated. Similarly, ? indicates that the effects of SP-IR axons on the target are not clear.

REFERENCES

1. Ai, J., D. Gozal, et al. (2007). "Degeneration of vagal efferent axons and terminals in cardiac ganglia of aged rats." J Comp Neurol **504**(1): 74-88.

2. Ai, J., R. D. Wurster, et al. (2009). "Vagal afferent innervation and remodeling in the aortic arch of young-adult fischer 344 rats following chronic intermittent hypoxia." Neuroscience **164**(2): 658-66.

3. Ambepityia, G., P. G. Kopelman, et al. (1990). "Exertional myocardial ischemia in diabetes: a quantitative analysis of anginal perceptual threshold and the influence of autonomic function." J Am Coll Cardiol **15**(1): 72-7.

4. Becker, D. E., H. Ancin, et al. (1996). "Automated 3-D montage synthesis from laser-scanning confocal images: application to quantitative tissue-level cytological analysis." Cytometry **25**(3): 235-45.

5. Benemei, S., P. Nicoletti, et al. (2009). "CGRP receptors in the control of pain and inflammation." Curr Opin Pharmacol **9**(1): 9-14.

6. Bolli, R. and A. Abdel-Latif (2005). "No pain, no gain: the useful function of angina." Circulation **112**(23): 3541-3.

7. Chang, Y., S. R. Stover, et al. (2001). "Regional localization and abundance of calcitonin gene-related peptide receptors in guinea pig heart." J Mol Cell Cardiol **33**(4): 745-54.

8. Cheng, Z., T. L. Powley, et al. (1997). "Vagal afferent innervation of the atria of the rat heart reconstructed with confocal microscopy." J Comp Neurol **381**(1): 1-17.

9. Cheng, Z., T. L. Powley, et al. (1997). "A laser confocal microscopic study of vagal afferent innervation of rat aortic arch: chemoreceptors as well as baroreceptors." J Auton Nerv Syst **67**(1-2): 1-14.

10. Cheng, Z., H. Zhang, et al. (2004). "Differential control over postganglionic neurons in rat cardiac ganglia by NA and DmnX neurons: anatomical evidence." Am J Physiol Regul Integr Comp Physiol **286**(4): R625-33.

11. Cheng, Z. and T. L. Powley (2000). "Nucleus ambiguus projections to cardiac ganglia of rat atria: an anterograde tracing study." J Comp Neurol **424**(4): 588-606.

12. Collins, T. J. (2007). "ImageJ for microscopy." Biotechniques **43**(1 Suppl): 25-30.

13. Faerman, I., E. Faccio, et al. (1977). "Autonomic neuropathy and painless myocardial infarction in diabetic patients. Histologic evidence of their relationship." Diabetes **26**(12): 1147-58.

14. Geppetti, P., R. Nassini, et al. (2008). "The concept of neurogenic inflammation." BJU Int **101 Suppl 3**: 2-6.

15. Gutterman, D. D. (2009). "Silent myocardial ischemia." Circ J **73**(5): 785-97.

16. Harden SW and Cheng ZJ (2009a). “Catecholaminergic Axon Distribution and Terminal Morphology in Whole-Mount Atria and Ventricles of Mice.” (Annual Meeting for Neuroscience Society, Chicago, #16751. Oct 17-21).

17. Harden SW and Cheng ZJ* (2009b). “Sympathetic and Parasympathetic Axon Distribution, Terminal Morphology, and Interaction in Whole-Mount Atria of Mice.” (Abstract, Annual Conference for Experimental Biology, April 17-22, 2010.)

18. Holzer, P. (1991). "Capsaicin: cellular targets, mechanisms of action, and selectivity for thin sensory neurons." Pharmacol Rev **43**(2): 143-201.

19. Holzer, P. and C. A. Maggi (1998). "Dissociation of dorsal root ganglion neurons into afferent and efferent-like neurons." Neuroscience **86**(2): 389-98.

20. Hoover, D. B. and J. C. Hancock (1988). "Distribution of substance P binding sites in guinea-pig heart and pharmacological effects of substance P." J Auton Nerv Syst **23**(3): 189-97.

21. Hoover, D. B., Y. Chang, et al. (2000). "Actions of tachykinins within the heart and their relevance to cardiovascular disease." Jpn J Pharmacol **84**(4): 367-73.

22. Hoover, D. B., A. V. Shepherd, et al. (2008). "Neurochemical diversity of afferent neurons that transduce sensory signals from dog ventricular myocardium." Auton Neurosci **141**(1-2): 38-45.

23. Hoover, D. B., E. R. Isaacs, et al. (2009). "Localization of multiple neurotransmitters in surgically derived specimens of human atrial ganglia." Neuroscience **164**(3): 1170-9.

24. Langer, A., M. R. Freeman, et al. (1991). "Detection of silent myocardial ischemia in diabetes mellitus." Am J Cardiol **67**(13): 1073-8.

25. Li, D., N. S. Li, et al. (2008). "Calcitonin gene-related peptide-mediated cardioprotection of postconditioning in isolated rat hearts." Regul Pept **147**(1-3): 4-8.

26. Li, L., C. Huang, et al. "Structural remodeling of vagal afferent innervation of aortic arch and nucleus ambiguus (NA) projections to cardiac ganglia in a transgenic mouse model of type 1 diabetes (OVE26)." J Comp Neurol **518**(14): 2771-93.

27. Lin, M., J. Ai, et al. "Impairment of baroreflex control of heart rate and structural changes of cardiac ganglia in conscious streptozotocin (STZ)-induced diabetic mice." Auton Neurosci **155**(1-2): 39-48.

28. Lin, M., J. Ai, et al. (2008). "Structural remodeling of nucleus ambiguus projections to cardiac ganglia following chronic intermittent hypoxia in C57BL/6J mice." J Comp Neurol **509**(1): 103-17.

29. Maggi, C. A. (1995). "Tachykinins and calcitonin gene-related peptide (CGRP) as co-transmitters released from peripheral endings of sensory nerves." Prog Neurobiol **45**(1): 1-98.

30. Mousa, S. A., M. Shaqura, et al. (2010) "Identification of mu- and kappa-opioid receptors as potential targets to regulate parasympathetic, sympathetic, and sensory neurons within rat intracardiac ganglia." J Comp Neurol **518**(18): 3836-47.

31. Pan, H. L. and S. R. Chen (2002). "Myocardial ischemia recruits mechanically insensitive cardiac sympathetic afferents in cats." J Neurophysiol **87**(2): 660-8.

32. Pan, H. L. and S. R. Chen (2004). "Sensing tissue ischemia: another new function for capsaicin receptors?" Circulation **110**(13): 1826-31.

33. Parsons, R. L. and D. S. Neel (1987). "Distribution of calcitonin gene-related peptide immunoreactive nerve fibers in the mudpuppy cardiac septum." J Auton Nerv Syst **21**(2-3): 135-43.

34. Parsons, R. L., S. A. Locknar, et al. (2006). "Presence and co-localization of vasoactive intestinal polypeptide with neuronal nitric oxide synthase in cells and nerve fibers within guinea pig intrinsic cardiac ganglia and cardiac tissue." Cell Tissue Res **323**(2): 197-209.

35. Richardson, R. J., I. Grkovic, et al. (2003). "Immunohistochemical analysis of intracardiac ganglia of the rat heart." Cell Tissue Res **314**(3): 337-50.

36. Saito, A., S. Kimura, et al. (1986). "Calcitonin gene-related peptide as potential neurotransmitter in guinea pig right atrium." Am J Physiol **250**(4 Pt 2): H693-8.

37. Schmidt, R. E., C. A. Parvin, et al. (2008). "Synaptic ultrastructural alterations anticipate the development of neuroaxonal dystrophy in sympathetic ganglia of aged and diabetic mice." J Neuropathol Exp Neurol **67**(12): 1166-86.

38. Seybold, V. S. (2009). "The role of peptides in central sensitization." Handb Exp Pharmacol(194): 451-91.

39. Shoba, T. and S. S. Tay (2000). "Nitrergic and peptidergic innervation in the developing rat heart." Anat Embryol (Berl) **201**(6): 491-500.

40. Song, J. X., L. H. Wang, et al. (2009). "Impaired transient receptor potential vanilloid 1 in streptozotocin-induced diabetic hearts." Int J Cardiol **134**(2): 290-2.

41. Thevenaz, P. and M. Unser (2007). "User-friendly semiautomated assembly of accurate image mosaics in microscopy." Microsc Res Tech **70**(2): 135-46.

42. Thornton, E., J. M. Ziebell, et al. "Kinin receptor antagonists as potential neuroprotective agents in central nervous system injury." Molecules **15**(9): 6598-618.

43. Wang, L. and D. H. Wang (2005). "TRPV1 gene knockout impairs postischemic recovery in isolated perfused heart in mice." Circulation **112**(23): 3617-23.

44. Wei, Z., L. Wang, et al. (2009). "Decreased expression of transient receptor potential vanilloid 1 impaires the postischemic recovery of diabetic mouse hearts." Circ J **73**(6): 1127-32.

45. Willis, W. D. and R. E. Coggeshall (1991). Structure of the Dorsal Horn. In Willis, W. D. and R. E. Coggeshall (Eds): Sensory mechanisms of the spinal cord. Second Edition, New York, Plenum Press, pp. 79-148.

46. Zahner, M. R., D. P. Li, et al. (2003). "Cardiac vanilloid receptor 1-expressing afferent nerves and their role in the cardiogenic sympathetic reflex in rats." J Physiol **551**(Pt 2): 515-23.

47. Zhong, B. and D. H. Wang (2008). "N-oleoyldopamine, a novel endogenous capsaicin-like lipid, protects the heart against ischemia-reperfusion injury via activation of TRPV1." Am J Physiol Heart Circ Physiol **295**(2): H728-35.